Blood flow cooling and ultrasonic lesion formation

Michael C. Kolios, Michael D. Sherar, and John W. Hunt
Department of Medical Biophysics, University of Toronto and Princess Margaret Hospital/Ontario Cancer Institute, Toronto, Ontario M5G 2M9, Canada

(Received 28 June 1995; accepted for publication 13 December 1995)

This article examines lesion formation using focused ultrasound and demonstrates how blood flow may affect lesion dimensions using a theoretical model. The effects of blood flow on temperature distributions during ultrasonic lesioning are examined for both regional cooling by the microvasculature and localized cooling due to thermally significant vessels. Regional cooling was critically assessed using two models: the Pennes bioheat transfer equation and the scalar effective thermal conductivity equation. Localized cooling was modeled by adding an advective term in the heat diffusion equation in regions enclosed by thermally significant vessels. A finite difference approach was used to solve the basic equations of heat transfer in perfused tissues in cylindrical coordinates. The extent of the lesioned tissue was determined by the accumulated thermal dose at each location. The size of the lesion was then calculated from the boundaries of the thermal isodose curves generated by the simulations. The results were compared to published *in vivo* lesion data in rat liver. It was shown that even for short ultrasound exposure times (~8 s), blood flow may play an important role in the thermal dose distribution. © *1996 American Association of Physicists in Medicine.*

Key words: ultrasonic lesioning, bioheat transfer, large vessel cooling

I. INTRODUCTION

Focused ultrasound has been used to produce lesions in tissues for the treatment of various pathologies.[1–3] The advent of imaging modalities that can image tissue damage in real time together with the better understanding of the interaction of ultrasound with tissues has renewed interest in ultrasound surgery. It has been postulated that the primary mechanism of lesion damage is thermal in nature.[4–7] Therefore, to characterize lesion formation, accurate thermal models are required that calculate the transient temperature distributions reached during the insonication. Knowledge of the time-temperature history of the tissues can be used to predict the extent of lesion formation. Blood flow may play an important role since it can have strong cooling effects in the heated field. This article is an extension of work done previously to predict lesion formation using focused ultrasound and thermal criteria for lesion onset.[8,9] The primary aim of this article is to examine how blood flow affects lesion dimensions.

Work from the field of hyperthermia has shown that blood flow cooling can be divided into the highly localized cooling by individual large vessels traversing heated volumes and microvascular cooling that occurs over larger tissue scales. The localized cooling by thermally significant vessels ($\delta > \sim 0.2$ mm) can usually be adequately modeled by a forced convection term in the regions of blood flow. Smaller sized vessels, due to their number and complex geometry, cannot be accounted for individually. To account for these vessels, the contributions of many blood vessels are averaged in order to predict a local average temperature.[10] Two such models have been used in hyperthermia treatment planning: the Pennes bioheat transfer equation (BHTE)[11] and the scalar effective thermal conductivity equation (ETCE).[12,13] The BHTE assumes that blood reaches the capillaries at the temperature of the supply vessels and thermally equilibrates with the surroundings instantaneously. The blood exits the veins at the local average temperature. Microvascular flow thus acts as a heat sink in this model. The ETCE model assumes that blood equilibration occurs at higher levels of the circulation, and that the collective effect of these vessels can be modeled as an enhanced conductivity of tissue. Under certain conditions, the effective conductivity tensor can be simplified to a scalar. A review of existing models can be found in Arkin *et al.*[14] Recent experimental data supports both models mentioned.[15,16]

Few studies[9,17] address the problem of blood flow cooling during ultrasonic lesion formation and none compare thermal model predictions of the BHTE and ETCE. In this work, the effects of blood flow on temperature distributions during ultrasonic surgery are examined for the regional cooling by the microvasculature (using the BHTE and ETCE models) and localized cooling of thermally significant vessels. Based on the time-temperature curves, predictions are made as to the extent of the lesioned tissue. The predictions using the BHTE and ETCE are compared using published coefficients for volumetric perfusion and effective conductivity.[18] Lesion dimensions are then compared to published *in vivo* rat liver data in experiments with and without blood flow to the organ.[19] Furthermore, novel thermal models[20] are used to predict time-temperature profiles near large blood vessels. These models provide better approximations to the temperature profiles near large vessels that have been used previously, especially for transient calculations.

 0094-2405/96/23(7)/1287/12/$10.00

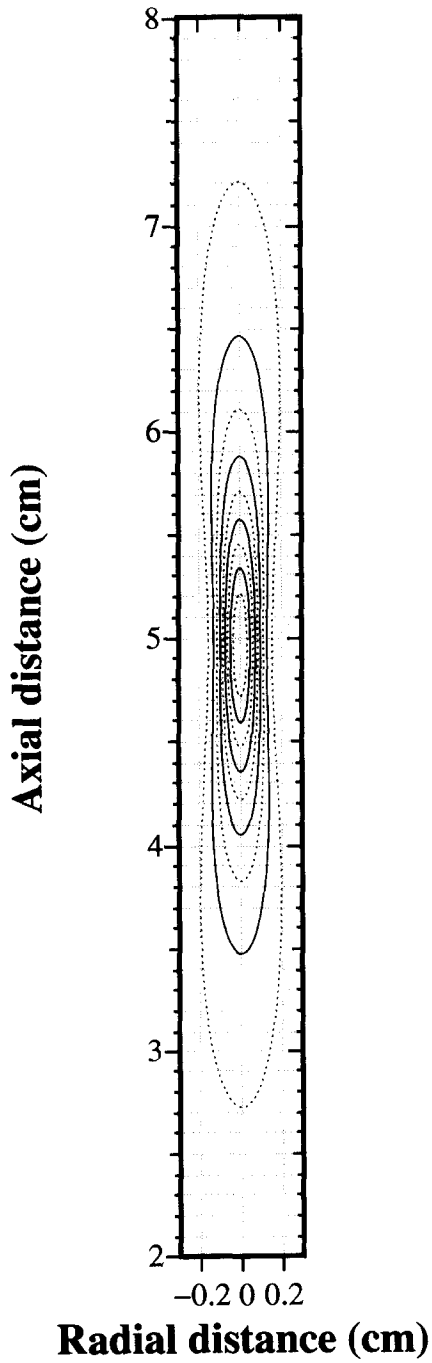

FIG. 1. Intensity pattern contours for the transducer used in the simulations (10% contour lines). The focal length of the 10 cm diam 1.7 MHz transducer is 14 cm and has a full-width half pressure maximum of ~2.4 mm.

II. METHODS

A. Ultrasound field calculations

At each computational node, the tissue power absorption was calculated based on the ultrasonic intensity profile. The Wu and Du Gaussian beam model[21] was used to estimate intensity patterns of the focused ultrasound applicators. For the case of cylindrical symmetry, the equations are

TABLE I. List of ultrasonic parameters used in simulations.

Transducer frequency (MHz)	1.7
Transducer radius of curvature (cm)	14
Transducer diameter (cm)	10
Intensity absorption coefficient (Np/cm)	0.2
Attenuation coefficient (Np/cm)	0.2

$$I(r',z')=\frac{8W_0}{\pi D_0^2}A(z')e^{-2\eta z'}e^{(-8Ar'^2)/D_0^2}, \tag{1}$$

$$A(z')=\frac{B}{\left(\frac{Bz'}{r_0}\right)^2+(1-z'/R)^2}. \tag{2}$$

The calculated normalized intensity pattern of the ultrasonic transducer used in these simulations is shown in Fig. 1. This simple formulation was used for rapid calculation of the acoustic fields, and ignores intensity side lobes that are formed by the ultrasound transducers. However, good agreement was found when this model was used to predict temperature elevation in a tissue equivalent phantom.[22] The volumetric power deposition was derived by multiplying the intensity with the tissue absorption coefficient:

$$P(r,z)=\mu I_{sp}(r,z)e^{-\eta z}. \tag{3}$$

It was assumed that all the attenuated power was absorbed and that the acoustic properties did not change during the insonication, thereby simplifying the problem. Experimental evidence, however, suggests a strong dependence of tissue attenuation with temperature, increasing with temperature,[23] and a significant increase in the tissue absorption coefficient for nonlesioned compared to lesioned tissue (by 100%–150%).[24] The acoustic properties used are listed in Table I. To compare the model predictions to experimental data of lesions formed on the rat liver surface,[19] the beam was focused 10 mm below the organ surface by assigning no ultrasonic absorption until 10 mm proximally to the focus. For the other simulations, the surface was located 3 cm away from the ultrasonic focus.

B. Temperature calculations

A finite difference algorithm was used to solve the BHTE and ETCE in cylindrical coordinates with or without a thermally significant vessel in the heated field. The geometry is given in Fig. 2. In brief, the equations solved were:

$$\rho_b c_b\frac{\partial T}{\partial t}+\rho_b c_b u(r)\frac{\partial T}{\partial z}=k_b\left(\frac{\partial^2 T}{\partial^2 r}+\frac{1}{r}\frac{\partial T}{dr}+\frac{\partial^2 T}{\partial^2 z}\right)+P_b, \quad \text{vessel domain} \tag{4}$$

$$\rho_t c_t\frac{\partial T}{\partial t}=k_{\text{eff}}\left(\frac{\partial^2 T}{\partial^2 r}+\frac{1}{r}\frac{\partial T}{dr}+\frac{\partial^2 T}{\partial^2 z}\right)-w_b c_b(T(r,z)-T_{\text{art}})+P_t, \quad \text{tissue domain.} \tag{5}$$

The vessel domains are modeled by Eq. (4), and the tissue regions are modeled by Eq. (5). The second term on the left

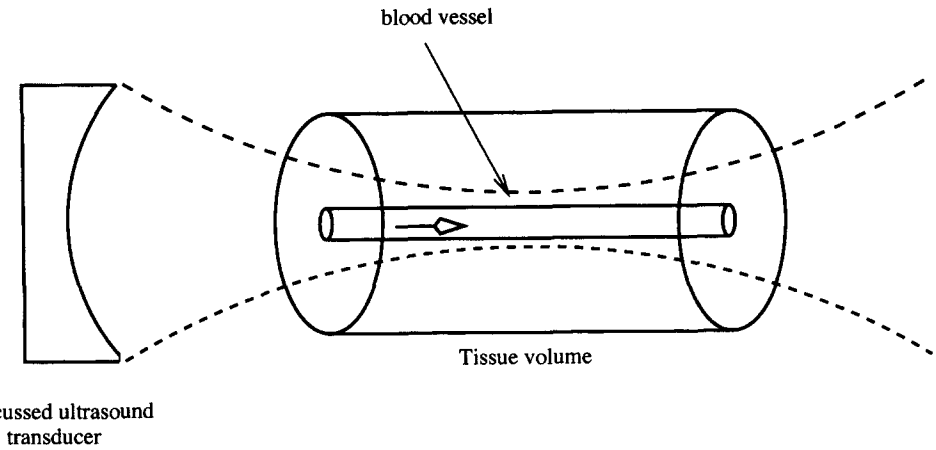

FIG. 2. The geometry of the simulations (cylindrical geometry). A focused ultrasound transducer insonicates perfused tissue with a vessel located at the center.

hand side of Eq. (4) is the advective term that models heat transport due to the mass transport of blood. The spacing in the axial direction dz was 1 mm while in the radial direction, the grid spacing dr varied linearly from 3.6 10^{-4} to 0.2 mm. The computational domain was 10 cm in the axial direction and 4 cm in the radial direction. The outer radial boundary and the face of the cylinder ($z=0$ cm) were set to a constant temperature while an adiabatic condition was implemented at the cylinder end ($z=10$ cm). Details on the numerical scheme can be found elsewhere.[20,25]

For simulations with no large vessels, Eq. (5) was solved. The BHTE was modeled by setting $k_{\text{eff}}=k_t$ in Eq. (5) and adjusting w_b to the value of interest (for the rat liver ~200–250 ml/100g/min).[19] In the simulations the value of 240 ml/100 g/min (0.04 g/cm^3/s) was used. Similarly, for the ETCE model, the second term on the right hand side of Eq. (5) is set to zero and k_{eff} assigned an equivalent value according to the experimental data of Crezee:[16]

$$k_{\text{eff}}=k_t(1+\alpha w_b), \tag{6}$$

where $\alpha=0.12$ (ml/100 g/min)$^{-1}$. Perfusion values were converted from ml/100 g/min to g/cm^3/s by dividing by 6000, assuming a tissue density of 1 g/cm^3. Thus, for a tissue perfusion of 240 ml/100 g/min (0.04 g/cm^3/s) the effective conductivity is ~29 times greater than the intrinsic conductivity of tissue. It was assumed that thermal properties and blood flow did not change during the insonication (listed in Table II). The power deposition was calculated by Eq. (3). In the vessel region, [Eq. (4)], it was assumed that the velocity profile was parabolic and that absorption of ultrasound by the blood was 10% of that for tissue.[26]

TABLE II. List of physical parameters used in temperature calculations.

Tissue/blood specific heat capacity (J/g/°C)	4.18
Tissue/blood density (g/cm^3)	1
Tissue/blood conductivity (W/cm/°C)	0.006
Blood perfusion (g/cm^3/s)	0–0.04

C. Lesion criteria

In vitro[27] and *in vivo*[28] data have demonstrated that the time required to produce a thermal isoeffect is decreased by a factor of two when the temperature is elevated by 1 °C for temperatures above 43 °C. This holds for tissue necrosis as the endpoint. A thermal dose can be defined as that which relates the time (t) required to produce an isoeffect (e.g., 3 logs of cell kill) at temperature T to the equivalent time (TD_{43}) which would be required to produce the same effect at 43 °C:[29,27]

$$TD_{43}=\sum_{t=t_0}^{t_{\text{end}}} 2^{T(t)-43}\Delta t, \quad T>=42.5\ ^\circ C\ \text{(min)}, \tag{7}$$

$$TD_{43}=\sum_{t=t_0}^{t_{\text{end}}} 2^{-0.5}6^{T(t)-42.5}\Delta t, \quad T<42.5\ ^\circ C\ \text{(min)}. \tag{8}$$

According to the above formulation, heating tissues to 43 °C for 120 min is equivalent to heating to ~56 °C for 1 s. This formula has been verified for temperatures up to 57 °C[30,28] and has been successfully used in predicting ultrasonic lesion size *in vivo*.[9]

In this work, tissue exposed for more than the equivalent of 60 min at 43 °C was considered *lesioned*. This is roughly equivalent to 3 logs of cell kill in a typical cell survival experiment and has been shown to induce tissue necrosis *in vivo*.[28] The size of the lesion was then calculated from the boundaries of the thermal isodose curves generated by the simulations. While tissues in general have a different TD_{43} to induce tissue necrosis, it is assumed here that the tissues are homogeneous and that the threshold is the same throughout the region of interest.

III. RESULTS

For a typical insonication, the time-temperature curves at the focal point are shown in Fig. 3(a). The *in situ* intensity level I_{SAL} used in the simulations was 100 W/cm^2 (equivalent to a peak intensity of 180 W/cm^2), where I_{SAL} is the spatially averaged focal intensity.[8,31] A sharp temperature

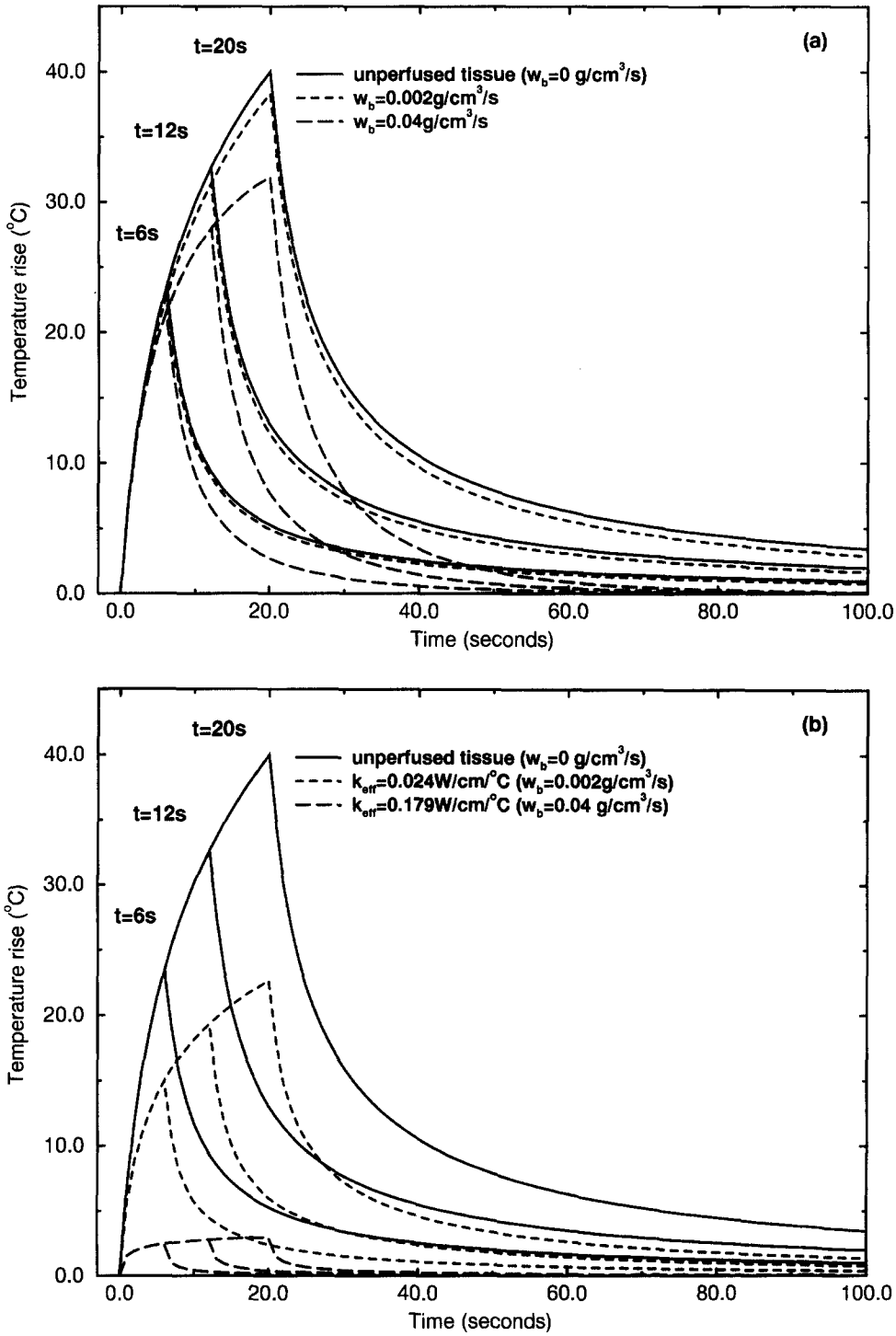

FIG. 3. Time-temperature profiles at focus for a 6, 12, and 20 s insonication (180 W/cm^2 peak intensity) for (a) the BHTE and (b) the ETCE. In (a), temperature profiles for no perfusion (solid line), a perfusion of 0.002 g/cm^3/s or a perfusion of 0.04 g/cm^3/s while in (b) profiles for no perfusion (solid line), an effective conductivity of 0.024 W/cm/°C (dashed line) or an effective conductivity of 0.179 W/cm/°C (long dashed line). Equivalent perfusion values derived from experimental data (Ref. 16).

rise is followed by a decline immediately after the ultrasound is turned off. A significant portion of the thermal dose is delivered after the transducer is turned off, and thus the temperature decay is critical to the accumulated thermal dose. For the power levels used in this example, the maximum temperature reached is approximately 70 °C without flow. For tissue perfusions comparable to liver (~200–250 ml/100 g/min), the temperature profiles are modified. The BHTE predicts a small reduction in the temperatures profiles [in Fig. 3(a)]. According to the ETCE, however, the maximum temperature rise for highly perfused tissues reached a maximum temperature of only 40 °C due to the high tissue effec-

TABLE III. Accumulated thermal dose at focal points (equivalent min at 43 °C TD_{43}) in temperature calculations of Figs. 3(a) and 3(b).

Exposure time (s)	w_b(g/cm^3/s)		k_{eff}(W/cm/°C)	
	w_b=0	w_b=0.04	k_{eff}=0.024	k_{eff}=0.179
t=6	3200	811	12.6	~0
t=12	2.6×10^6	1.3×10^5	380	~0
t=20	6.0×10^8	3.8×10^6	6246	~0

tive conductivity [in Fig. 3(b)]. For perfusion values comparable to liver perfusion and according to Eq. (6), the ETCE does not predict the formation of lesions due to the low temperatures (and thus thermal dose) reached. Table III illustrates the accumulated thermal dose at the focal point based on the temperature profiles presented in Figs. 3(a) and 3(b). Hence, further analysis of thermal dose distributions will be based on the BHTE predictions since the ETCE does not predict lesions formed for high effective conductivities.

Thermal dose isocontours are plotted in Fig. 4. The region enclosed in the thermal dose isocontour of 60 min at 43 °C (TD_{43}=60 min) is defined as the lesioned tissue. The lesion formed closely follows the intensity pattern at the focus (in Figs. 1 and 4). Furthermore, the cigar-shaped lesion formed agrees well with experimental observations.[19] The thermal dose gradients are steep and well-defined and, hence, lesion dimensions are relatively insensitive to variabilities in lesion thresholds of various tissues. Figure 5(a) illustrates that a lesion threshold thermal dose of 60 min at 43 °C (TD_{43}=60 min) defines a 2.4 mm diam lesion while the isocontour for 300 min at 43 °C (TD_{43}=300 min) is 2.0 mm diam (in this example for no perfusion and organ surface 3 cm from focal depth). This represents a 16% change. A similar change in lesion length is demonstrated in Fig. 5(b). It should be noted that this range of thresholds is large and unlikely to be encountered in tissues. The factor of 2 in Eqs. (7) and (8) for the thermal dose, however, may vary depending on tissue type,[27] and its effects on ultrasonic lesion size have been described elsewhere.[32]

A comparison of the predicted lesion diameters with published experimental data[19] demonstrates reasonable agreement (Fig. 6). The physical parameters used (Tables I and II) were chosen to match the experimental conditions. No large vessel effects were included in these simulations. For the case of no perfusion the experimental data (solid squares) and theoretical predictions (long-dashed line) agree fairly well, apart for short insonication times. With perfusion, the agreement is worse, however, the curve trends are similar. There again are discrepancies for short exposure times.

An increase of perfusion according to the BHTE reduces the lesion size. The reduction in size depends on the insonication time and blood flow. Longer duration insonications allow the effects of both blood flow and thermal conduction to alter the temperature profiles. Figure 7 plots lesion diameter and length versus volumetric tissue perfusion for three exposure times: 2, 8, and 12 s. Ultrasonic intensity was adjusted to create lesions of approximately the same size when

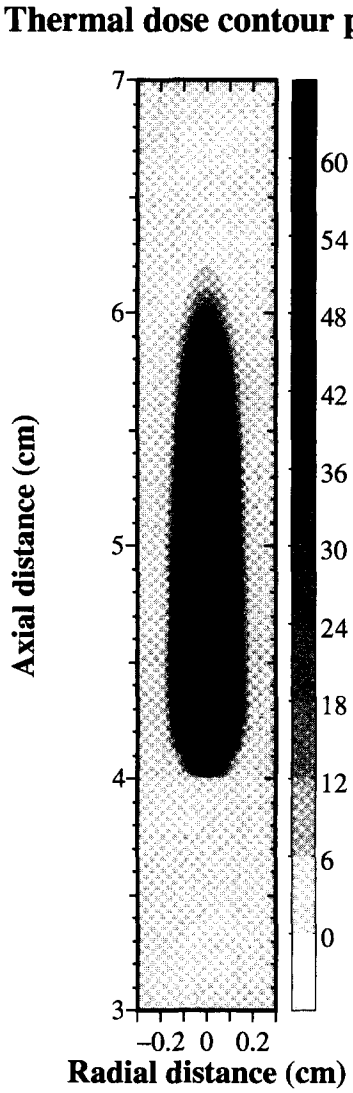

FIG. 4. Thermal dose (TD_{43}) contour plot for a 12 s insonication with no perfusion (10% contour lines, maximum TD_{43} of 60 min). Note the sharp thermal dose gradients created. This indicates that the lesions formed will have well defined boundaries.

there was no perfusion. While there is minimal reduction in lesion diameter for the 2 s exposure for all perfusion values (maximum of ~5%), for the 12 s exposure the reduction is significant (~30%) for high perfusion values (comparable to that of the human kidney). The results are similar for lesion length.

The effects of large vessels on lesion formation were examined by including the adjective term [Eq. (4)] in the finite difference algorithm for regions enclosed by the large vessel (Fig. 2). Various vessel diameters (Table IV) were examined for a 12 s exposure at 180 W/cm^2 peak intensity *in situ* and results are shown in Fig. 8. Depending on the vessel size and the dimensions of the ultrasonic beam, the lesion shape and size can be significantly altered. For vessels greater than 0.5 mm diam and for the intensity profile of Fig. 1, the lesion is separated in two halves that surround the blood vessel forming a cylindrical shell of nonlesioned tissue. For vessels

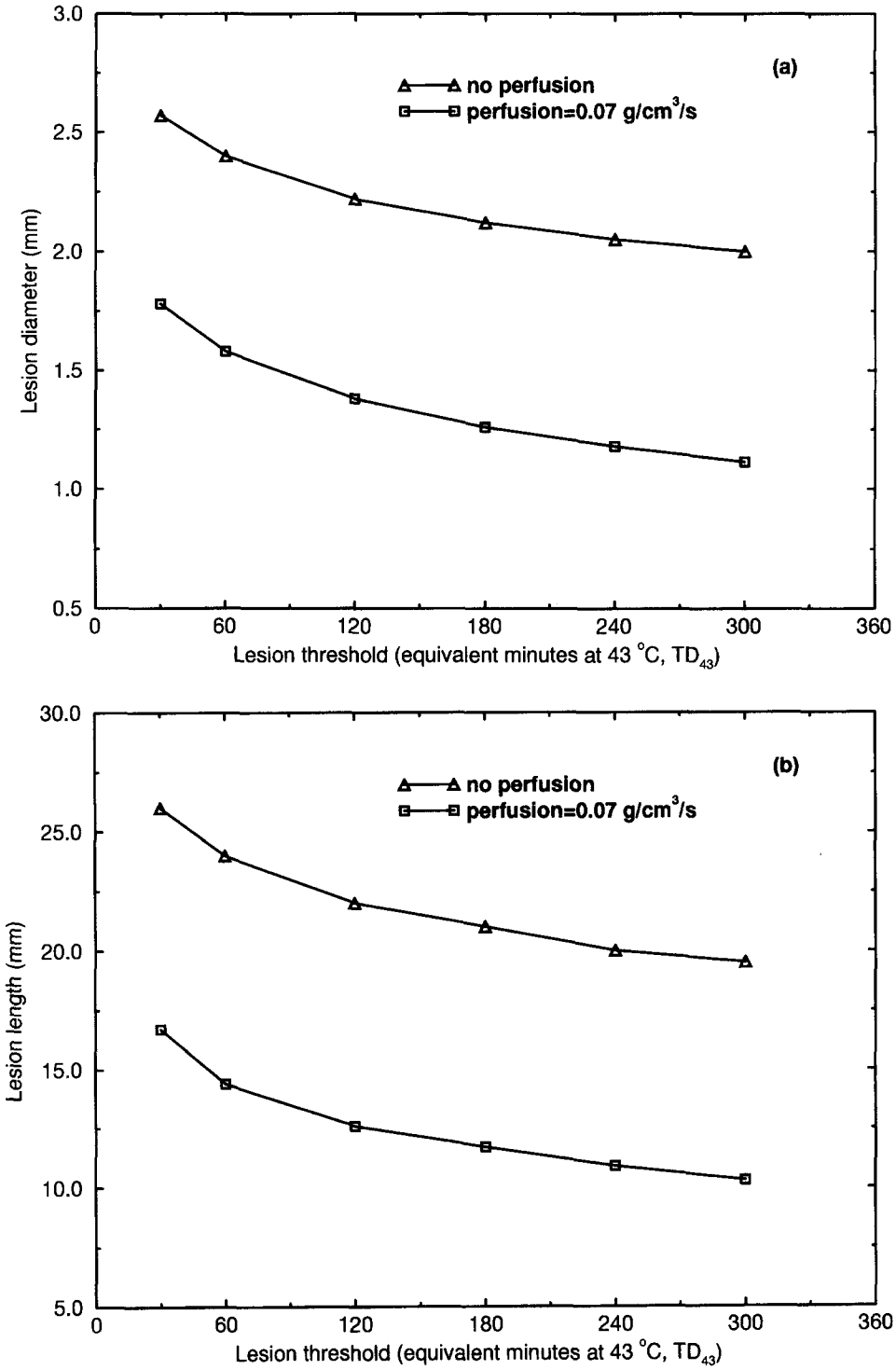

FIG. 5. Lesion diameter (a) and lesion length (b) plotted against lesion threshold for a 12 s (180 W/cm^2 peak intensity) insonication for no perfusion and high perfusion.

larger than 1 mm diam, a lesion is not formed since the majority of energy is deposited in the blood vessel which has low ultrasonic absorption and carries the heat away. Transfer of heat in the direction of the flow is detected for smaller vessels (diameter greater than 0.2 mm) elongating the lesioned tissue in the direction of the blood flow. This is assuming however that the blood flow is constant in the vessel during the entire sonication period.

The effect of volumetric flow on the lesion size was examined by modifying the average velocity of the 0.6 mm diam vessel to 2, 4, 6, 8 and 10 cm/s. Figure 9 illustrates that higher flow through the vessel reduces the lesion size and

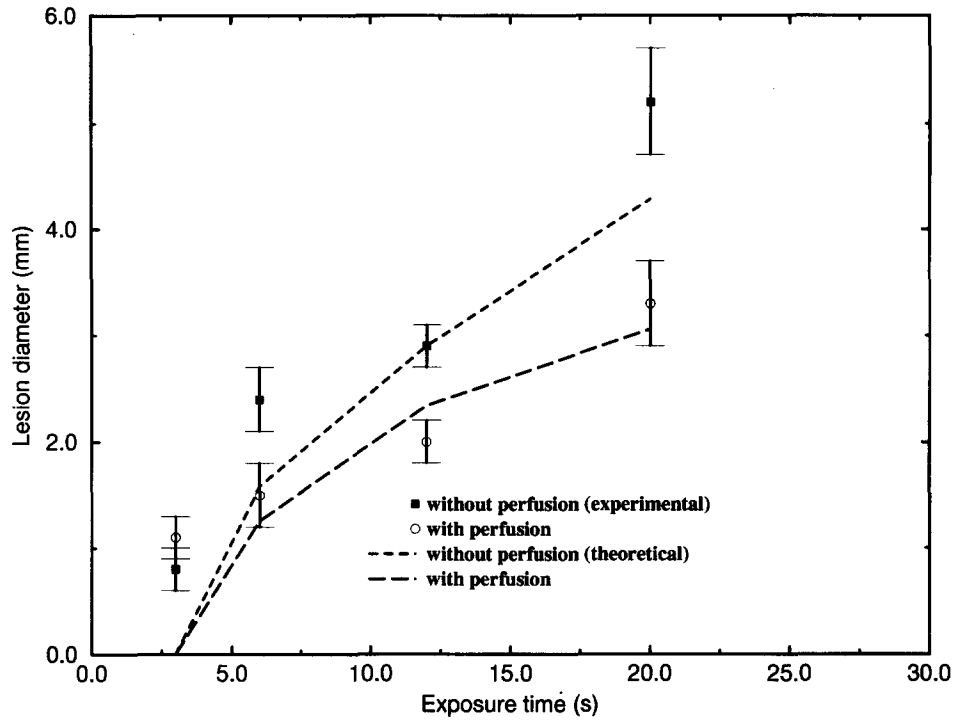

FIG. 6. Comparison of experimental data derived from rat liver (Ref. 19) with predicted values from thermal model calculations using the parameters listed in Tables I and II. Note the discrepancy at short exposure times.

distorts its shape. Lesion dimensions at the focal point as a function of average velocity through the blood vessel are tabulated in Table V (lesion length is difficult to define in this situation due to the lesion shape). It is clear that volumetric flow is an important determinant of the effects of large vessels. A closer examination of the radial thermal dose profiles at the focal depth for the 0.6 mm diam vessel demonstrates a thin layer of tissue (~0.18 mm) adjacent to the vessel wall that receives a thermal dose lower than the lesion threshold [Fig. 10(a)]. This would lead to tissue sparing during lesioning. An exposure time of 3 s, (400 W/cm^2 peak intensity) however, reduces tissue layer spared close to the vessel to ~0.06 mm [Fig. 10(b)]. Therefore, high power short duration pulses of the order of 1–3 s are required to minimize the effects of large vessels.

IV. DISCUSSION

Ultrasonic lesioning can be used to produce well defined lesions in depth in tissue as long as air cavities and bone are not in the beam path. Delayed inpart by the lack of noninvasive means to monitor ultrasonic surgery, new exciting developments in imaging have renewed interest in this modality.[1] If cavitation and acoustic propagation nonlinearities are avoided, the lesion size and shape can be well described by thermal considerations. For short exposures, the thermal dose gradients are very sharp and hence lesion dimensions are relatively insensitive to variation in the thermal sensitivity of various tissues (Fig. 5). Therefore, while a thermal dose of 60 min at 43 °C (approximately 3 logs of cell kill) might not be considered sufficient for lesioning tissues, lesion size does not change appreciably if higher dose thresholds are used. Furthermore, lesion size is not strongly dependent on the attenuation coefficient of tissues.[9] Therefore, for short exposure times, ultrasonic lesioning can be used for a variety of tissues with similar perfusion and thermal parameters without large differences in outcome expected.

Blood flow, however, can effect the temperature distributions and thus the lesion shape and size. For high perfusions lesions are not formed according to the predictions of the scalar ETCE model. The sharp temperature gradients created by the source and the high values of enhanced conductivity rapidly smear out the temperature rise. The low temperatures achieved restrict the thermal dose to nonlesioning levels. The effective conductivity values based on Eq. (6) might not be a good indicator of the effective conductivity in the rat liver experiments. However, high values of effective conductivity have been reported elsewhere[33,34] and, therefore, should be considered realistic. Since the ETCE model predictions do not agree with the lesions observed in the experimental data, it was not used for further analysis. The ETCE model may be useful in tissues with low perfusions or where the vascular architecture satisfies appropriate conditions.[35]

A perfusion increase according to the BHTE reduces the size of the lesions formed. For highly perfused tissues such as kidney and liver—even for short exposures (~8 s)—lesion size can be reduced by one third. Exposure times of 2 s are predicted to produce lesions whose size is independent of perfusion. This agrees well with recent experimental lesion data in rabbit brain[36] and with theoretical predictions of rapid heating for hyperthermia.[17,37] Therefore, short expo-

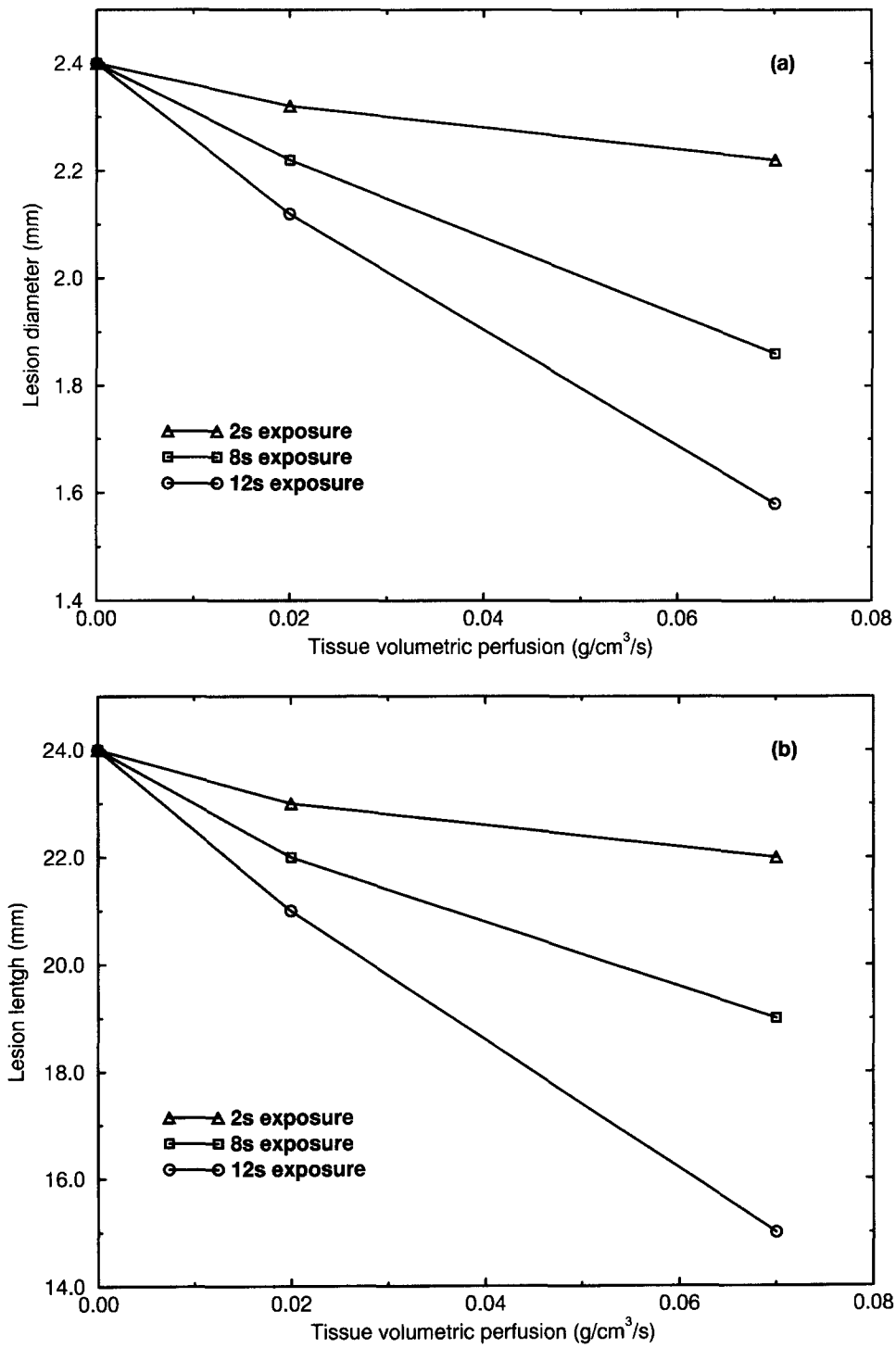

FIG. 7. Perfusion dependence of (a) lesion diameter and (b) lesion length for three exposure times. As the exposure time increases, the effects of perfusion are greater. For very small exposure times (~2 s), lesion formation is almost perfusion independent.

sure times are required to minimize the effects of blood flow (Fig. 7). However, higher acoustic intensities are required to achieve this; therefore, phenomena such as cavitation, acoustic nonlinear propagation and other nonthermal mechanisms may contribute to tissue necrosis. These effects are not well understood and cannot be, at the present time, adequately quantified.[7] Hynynen *et al.*[31] recommended that peak intensities lower than 700 W/cm^2 at 1 MHz be used to avoid the unpredictable energy absorption or direct cytotoxicity of nonthermal effects. In the case of lower perfused tissues such as muscle (~8 ml/100 g/min), up to 12 s exposures could be used without reducing lesion diameter more than 10% (Fig. 7).

A comparison of the predicted lesion diameters with pub-

TABLE IV. Significant vessel diameters and average flow rates (Refs. 18 and 46). Vessel flow values linearly extrapolated for vessel diameters not found in references.

Blood vessel diameter (mm)	Average velocity
1.4	10.5 cm/s
1	8 cm/s
0.8	7.5 cm/s
0.6	6.0 cm/s
0.4	5.5 cm/s
0.2	3.4 cm/s

lished experimental data demonstrate reasonable agreement. Differences can be attributed to uncertainties in the values of the physical parameters used in the simulations, or even their temperature dependence. Ultrasonic absorption may vary by 50%–100% in this temperature range.[24] The greatest discrepancy was detected for the short exposures. It was noted during the experiments that indirect damage might occur in the liver due to lack of blood supply after the insonication.[38,19] If the thermal dose threshold for vascular collapse is lower than that for lesioning, then a lesion might form due to the vascular collapse rather than direct heat cytotoxicity. Thermal dose thresholds for this effect in the mouse leg are of comparable magnitude to direct heat cytotoxicity.[39] A reduction in clearance rate of a radioactive tracer by 37%, taken as an indicator of microvascular integrity, had thresholds for TD_{43} of 83±7 and 173±30 min for tumor and muscle tissue, respectively. This effect, however, is predicted to be negligible

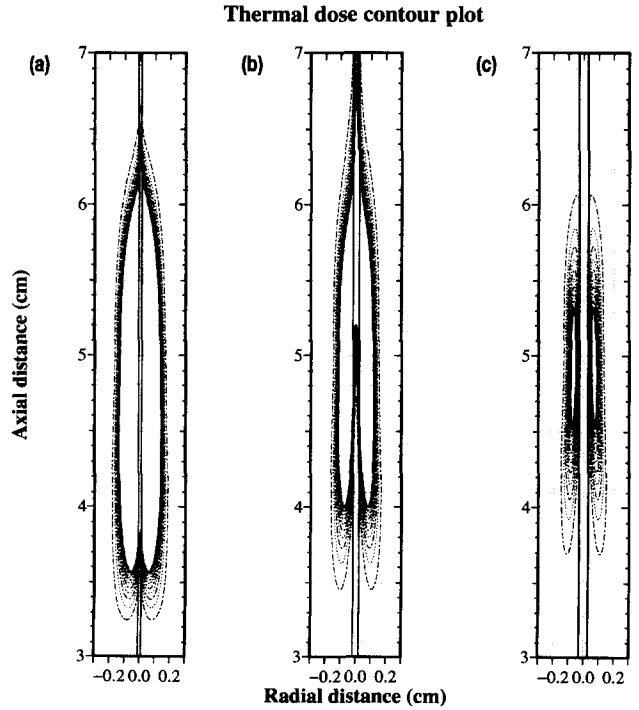

FIG. 8. Thermal dose contours for a 12 s (180 W/cm^2 peak intensity) insonication for an (a) 0.2 mm (b) 0.4 mm (c) 0.6 mm vessel. Flow velocities are given in Table IV. The inner solid line defines the lesion boundaries.

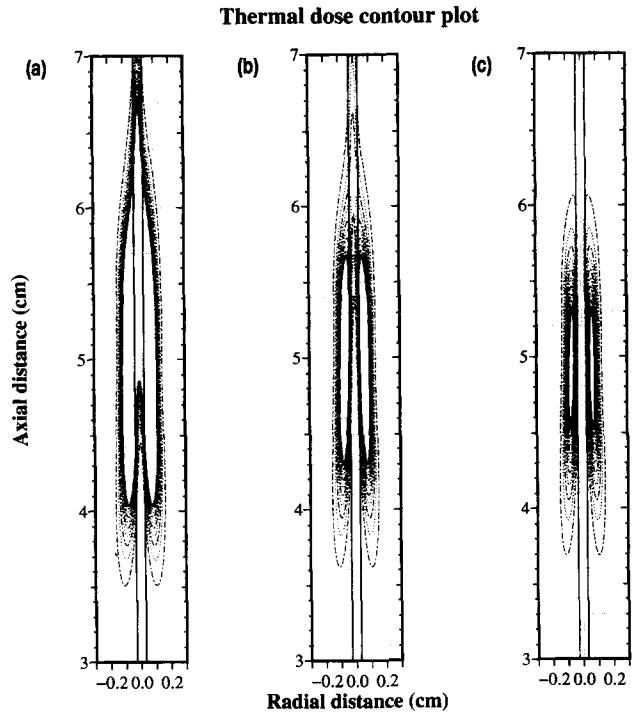

FIG. 9. Thermal dose contours for a 12 s (180 W/cm^2 peak intensity) insonication near a 0.6 mm vessel with (a) u_{avg}=2 cm/s (b) u_{avg}=4 cm/s (c) u_{avg}=6 cm/s.

at the boundaries of the lesion where the thermal gradients are steep (Fig. 5). While the thermal conductivity of tissue does not change appreciably in this temperature range,[26] thermal conductivity variations between tissue types should be considered. The lesion diameter and length in sample runs (12 s, 180 W/cm^2 insonication, no perfusion) for a tissue conductivity of 0.002 W/cm/°C (simulating fat) versus 0.006 W/cm/°C (simulating muscle) were 3.6, 33 and 2.6, 24 mm, respectively. Therefore, in tissues with low thermal conductivity, lesion size is expected to be larger than in other tissues with higher values.

In the clinical practice of moderate temperature hyperthermia, high temperature tissue lesioning and cryotherapy, it has been observed that tissues close to large vessels remain viable. When a 0.6 mm diam vessel is introduced in the center of the tissue, a layer of tissue close to the vessel receives a low thermal dose. Therefore, if destruction of all cells is required (as with the case for a malignancy), shorter exposures are required to minimize the viable rim around the

TABLE V. Outer and inner lesion boundaries around a 0.3 mm radius vessel at the focal depth.

Average velocity (cm/s)	Outer boundary (mm)	Inner boundary (mm)
0	1.3	N/A
2	1.15	N/A
4	1.00	0.33
6	0.86	0.48
8	No lesion	No lesion

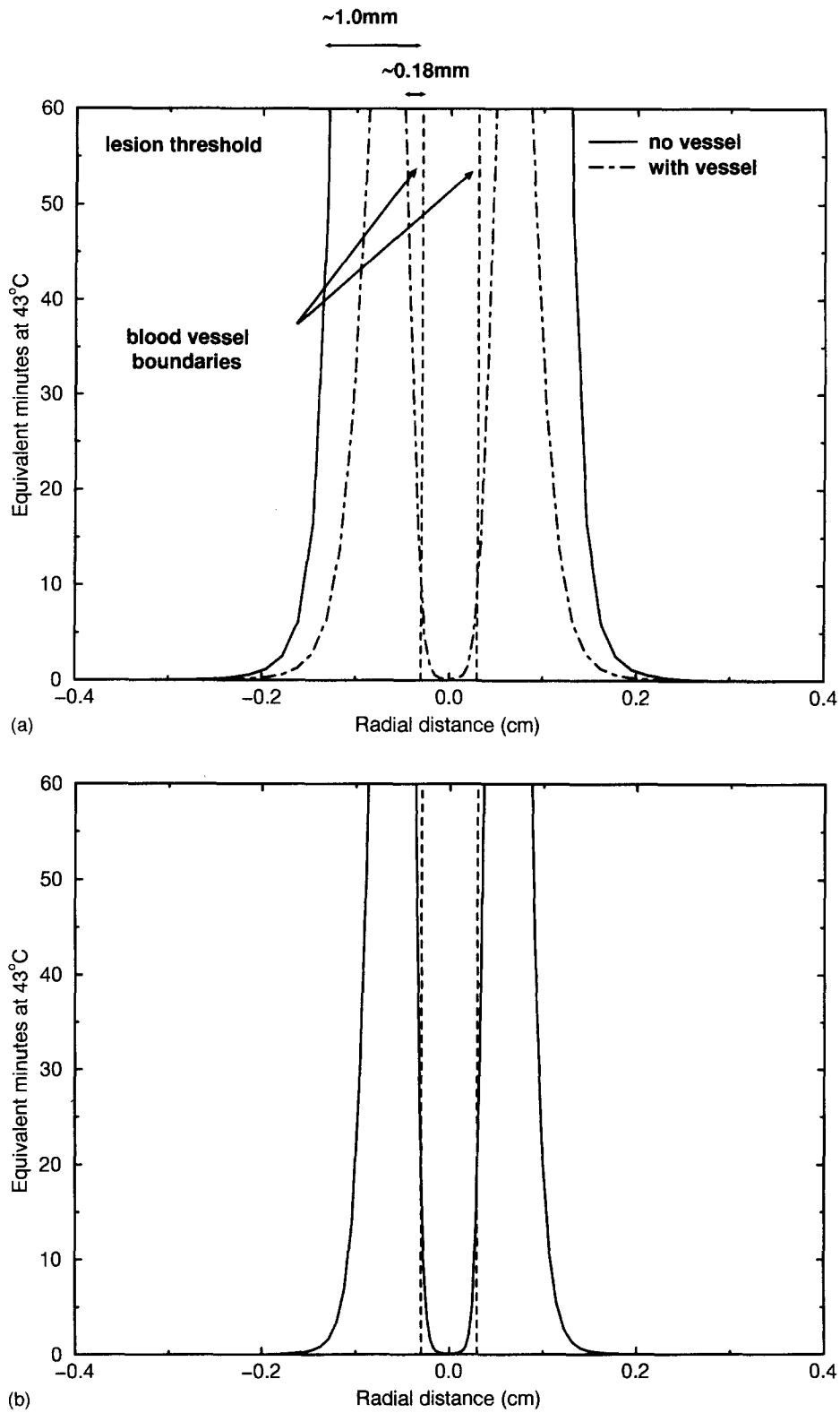

FIG. 10. Thermal dose plotted vs. radial distance at the focal depth in the presence of a 0.6 mm vessel (u_{avg}=6 cm/s) for an (a) 12 s insonication (b) a 3 s insonication. Note the volume of tissue adjacent to the vessel that is protected from thermal damage in (a) and how it is minimized in (b).

vessel. Even for exposures of ~2 s, however, a viable rim is predicted [Fig. 10(b)]. Similar conclusions were drawn in the experimental heating of large blood vessels *in vivo*.[40] There are instances when this effect is advantageous, protecting critical vessels from endothelial injury. One such example is in cardiac rf catheter ablation for which large coronary vessels are spared.[41] In this article, the vessel axis is parallel to the beam (Fig. 2). The results therefore maximize the cooling

effects of the vessels since they occupy a large fraction of the irradiated tissue. Three-dimensional thermal models are being developed in our laboratory to simulate more realistic vascular geometries.

Ultrasonically induced lesions are small in general. To treat large tissue volumes ultrasound lesioning techniques using multiple insonications,[42,43] focal pattern synthesis[44,45] or a combination of both are required to treat the entire volume. Treatment planning is particularly important in this case since intervening normal tissue might be damaged due to the accumulation of thermal dose resulting from the multiple exposures.[43] Furthermore, if the intensity field pattern overlaps existing lesioned tissue, this could lead to a change of the expected lesion size and shape.[38] This is termed lesion-to-lesion interaction and usually results in displacing the lesion (with respect to its location in the absence of another lesion) and reducing its size. Predicting *a priori* these effects with accurate thermal models would help to minimize normal tissue damage.

The thermal model used here is not limited to ultrasonic lesioning; it can be applied to other therapeutic modalities that depend on thermal cytotoxicity. Given a specific specific absorption rate (the SAR or absorbed power per unit mass) or conductive heating, the time-temperature curves can be collected and analyzed. Thus the models can be applied to applicator optimization, with lesion shape as the endpoint. Single or multiple applicators can be examined given their SAR which can either be measured experimentally or calculated theoretically. Finally, such models could assist in treatment planning by calculating thermal doses so as to maximize the dose in the target regions and minimize the dose to the surrounding healthy tissue.

V. CONCLUSIONS

Thermal models can be used to predict the shape and size of ultrasonically induced lesions. Blood flow can effect the shape and size of these lesions. Large vessels (>0.5 mm) create localized cool spots that spare tissue from thermal damage. Tissue microvascular perfusion becomes a factor for exposure times greater than 2 s for highly perfused tissues. While the BHTE equation predictions agreed with published experimental lesion data, the ETCE did not predict tissue lesioning for high values of perfusion.

ACKNOWLEDGMENTS

The authors would like to gratefully acknowledge the financial support of the National Cancer Institute of Canada and the Ontario Cancer Treatment and Research Foundation. The first author is also partially supported by a University of Toronto Open Doctoral Scholarship. Finally, the authors would like to thank Dr. Gail ter Haar and Dr. Lili Chen for fruitful discussions.

NOMENCLATURE

c =specific heat capacity (J/g/°C)
dr =grid spacing in the radial direction (cm)
dz =grid spacing in the axial direction (cm)
k =thermal conductivity (W/cm/°C)
k_{eff} =scalar effective conductivity of tissue (W/cm/°C)
r,z =radial and axial coordinates (cm)
$u(r)$ =velocity of blood (cm/s)
w =volumetric perfusion rate (g/cm^3/s)
P =volumetric power deposition rate (W/cm^3)
T =temperature (°C)
α =best fit parameter equating perfusion and effective conductivity (g/cm^3/s)$^{-1}$
δ =blood vessel diameter (cm)
ρ =density (kg/cm^3)
r_0 =Rayleigh distance (m)=$\pi D_0/4\lambda$
A =Gaussian coefficient at distance z'
B =Gaussian coefficient at distance $z'=0$
BHTE =Pennes bioheat transfer equation
D_0 =diameter of the transducer (cm)
ETCE =effective thermal conductivity equation
I =ultrasonic intensity (W/cm^2)
R =radius of curvature (cm)
SAR =specific absorption rate (W/cm^3)
TD_{43} =equivalent minutes at 43 °C (min)
W_0 =total acoustic power generated by the transducer (W)
η =ultrasonic intensity attenuation coefficient (Np/cm)
λ =ultrasonic wavelength (cm)
μ =ultrasonic intensity absorption coefficient (Np/cm)

subscripts
art=arterial
avg=average
sp=spatial peak
b=blood
t=tissue

[1]K. Hynynen, A. Darkazanli, C. A. Damianou, E. Unger, and J. F. Schenck, "The usefulness of a contrast agent and gradient-recalled acquisition in a steady-state imaging sequence for magnetic resonance imaging-guided noninvasive ultrasound surgery," Invest. Radiol. **29**, 897–903 (1994).
[2]H. E. Cline, J. F. Schenck, R. D. Watkins, K. Hynynen, and F. A. Jolesz, "Magnetic resonance-guided thermal surgery," Magn. Reson. Med. **30**, 98–106 (1993).
[3]G. ter Haar, I. Rivens, L. Chen, and S. Riddler, "High intensity focused ultrasound for the treatment of rat tumors," Phys. Med. Biol. **36**, 1495–501 (1991).
[4]J. B. Pond, "The role of heat in the production of ultrasonic focal lesions," J. Acoust. Soc. Am. **47**, 1607–1611 (1970).
[5]F. J. Fry, G. Kossoff, R. C. Eggleton, and F. Dunn, "Threshold ultrasonic dosages for structural changes in the mammalian brain," J. Acoust. Soc. Am. **48**, 1413–1417 (1970).
[6]R. M. Lerner, E. L. Carstensen, and F. Dunn, "Frequency dependence of thresholds for ultrasonic production of thermal lesions in tissue," J. Acoust. Soc. Am. **54**, 504–506 (1973).
[7]NCRP, "Exposure criteria for medical diagnostic ultrasound: I. criteria based on thermal mechanisms," Technical Report No. 113, National Council on Radiation Protection and Measurements, Bethesda, MD, 1992.
[8]C. R. Hill, I. Rivens, M. G. Vaughan, and G. R. ter Haar, "Lesion development in focused ultrasound surgery: A general model," Ultrasound in Med. Biol. **20**, 259–269 (1994).

[9]C. Damianou and K. Hynynen, "The effect of various physical parameters on the size and shape of necrosed tissue volume during ultrasound surgery," J. Acoust. Soc. Am. 95, 1641–1649 (1994).
[10]J. W. Baish, "Formulation of a statistical model of heat transfer in perfused tissue," J. Biomechan. Eng. **116**, 521 (1994).
[11]H. H. Pennes, "Analysis of tissue and arterial blood temperatures in the resting human *forearm*," J. Appl. Physiol. **1**, 93–122 (1948).
[12]J. J. W. Lagendijk, "Thermal models: principles and implementation," *Introduction to the Clinical Aspects of Clinical Hyperthermia*, edited by S. B. Field and J. W. Hand. (Taylor and Francis, Bristol, PA, 1990), pp. 478–511.
[13]S. Weinbaum, L. M. Jiji, and D. E. Lemons, "Theory and experiment for the effect of vascular microstructure on surface heat transfer—part I: Anatomical foundation and model conceptualization," J. Biochem. Eng. **106**, 321–330 (1984).
[14]H. Arkin, L. X. Xu, and K. R. Holmes, "Recent developments in modeling heat transfer in blood perfused tissues," IEEE Trans. Biomed. Eng. **41**, 97–107 (1994).
[15]E. G. Moros, A. W. Dutton, R. B. Roemer, M. Burton, and K. Hynynen, "Experimental evaluation of two simple thermal models using hyperthermia *in vivo*," Int. J. Hypertherm. 9, 581–598 (1993).
[16]J. Crezee and J. J. W. Lagendijk, "Experimental verification of bio heat transfer thoeries: measurement of temperature profiles around large artificial vessels in perfused tissue," Phys. Med. Biol. **35**, 905–923 (1990).
[17]B. E. Billard, K. Hynynen, and R. B. Roemer, "Effects of physical parameters on high temperature ultrasound hyperthermia," Ultrasound Med. Biol. **16**, 409–420 (1990).
[18]J. Crezee and J. J. W. Lagendijk, "Temperature uniformity during hyperthermia: The impact of large vessels," Phys. Med. Biol. **37**, 1321–1337 (1992).
[19]L. Chen, G. ter Haar, C. R. Hill, M. Dworkin, P. Carnochan, H. Young, and J. P. Bensted, "Effect of blood perfusion on the ablation of liver parenchyma with high-intensity focused ultrasound," Phys. Med. Biol. **38**, 1661–1673 (1993).
[20]M. C. Kolios, M. D. Sherar, and J. W. Hunt, "Large vessel cooling in heated tissues: A *numerical study*," Phys. Med. Biol. **40**, 477–494 (1995).
[21]J. R. Wu and G. H. Du, "Temperature rise in a tissue-mimicking material generated by unfocused and focused ultrasonic transducers," Ultrasound Med. Biol. **16**, 489–498 (1990).
[22]J. Wu, J. D. Chase, Z. Zhu, and T. P. Holzapfel, "Temperature rise in a tissue-mimicking material generated by unfocused and focused ultrasonic transducers," Ultrasound Med. Biol. **18**, 495–512 (1992).
[23]J. C. Bamber and C. R. Hill, "Ultrasonic attenuation and propagation speed in mammalian tissues as a function of temperature," Ultrasound Med. Biol. **5**, 149–157 (1979).
[24]N. L. Bush, I. Rivens, G. R. ter Haar, and J. C. Bamber, "Acoustic properties of lesions generated with an ultrasound therapy system," Ultrasound Med. Biol. **19**, 789–801 (1993).
[25]M. C. Kolios, M. D. Sherar, A. E. Worthington, and J. W. Hunt, "Modeling temperature gradients near large vessels in perfused tissues," In *Fundamentals of Biomedical Heat Transfer*, edited by M. A. Ebadian and P. H. Oosthuizen (American Society of Mechanical Engineers, New York, 1994), Vol. 295, pp. 23–30.
[26]F. A. Duck, *Physical Properties of Tissues: A Comprehensive Reference Book* (Academic, San Diego, 1990).
[27]S. A. Sapareto and W. C. Dewey, "Thermal dose determination in cancer therapy," Int. J. Radiat. Oncology. Biol. Phys. **10**, 787–800 (1984).
[28]C. A. Linke, W. Lounsberry, and V. Goldschmidt, "Localized heating of tissue by electric and nonelectric means," Invest. Urol. **4**, 586–599 (1967).
[29]G. P. Raaphorst, *Fundamental Aspects of Hyperthermic Biology* (Taylor and Francis, Bristol, 1990), p. 572.
[30]J. Borelli, L. L. Thompson, C. C. Cain, and W. C. Dewey, "Time-temperature analysis of cell killing of BHK cells heated at temperatures in the range of 43.5 °C to 57.0 °C," Int. J. Radiat. Oncology. Biol. Phys. **19**, 389–399 (1990).
[31]K. Hynynen, "The threshold for thermally significant cavitation in dog's thigh muscle *in vivo*," Ultrasoound Med. Biol. **17**, 157–169 (1991).
[32]C. A. Damianou, K. Hynynen, and X. Fan, "Evaluation of accuracy of a theoretical model for predicting the necrosed tissue volume during focused ultrasound surgery," IEEE Trans. Ultrason. Ferroelect. Frequency Control **42**, 182–187 (1995).
[33]A. W. Dutton, "A finite element solution to conjugated heat transfer in tissue using magnetic resonance angiography to measure the *in vitro* velocity field," Ph.D. thesis, University of Arizona, 1993.
[34]H. F. Bowman, M. G. Curley, W. H. Newman, S. C. Summit, S. Chang, J. Hansen, T. S. Herman, and G. K. Svensson, "Use of effective conductivity for hyperthermia treatment planning," in *Bioheat Transfer-Applications in Hyperthermia, Emerging Horizons in Instrumentation and modelling* edited by R. B. Roemer, J. J. McGrath, and H. F. Bowman (American Society of Mechanical Engineers, New York, 1989), pp. 23–28, HTD-126/BED-12.
[35]L. Zhu, D. E. Lemons, and S. Weinhaum, "A new approach for predicting the enhancement in the effective conductivity of perfused muscle tissue due to hyperthermia," Ann. Biomed. Eng. **23**, 1–12 (1995).
[36]N. I. Vykhodtseva, K. Hynynen, and C. Damianou, "Pulse duration and peak intensity during focused ultrasound surgery: Theoretical and experimental *effects* in rabbit brain *in vivo*," Ultrasound Med. Biol. **20**, 987–1000 (1994).
[37]J. W. Hunt, R. J. Lalonde, H. Ginsberg, S. Urchuck, and A. Worthington, "Rapid heating: critical theoretical assessments of thermal gradients found in hyperthermia treatments," Int. J. Hyperthermia, **7**, 703–718 (1991).
[38]L. Chen, I. Rivens, G. ter Haar, S. Riddler, C. R. Hill, and J. P. Bensted, "Histological changes in rat liver tumours treated with high-intensity focused ultrasound," Ultrasound Med. Biol. **19**, 67–74 (1993).
[39]S. L. Brown, J. W. Hunt, and R. P. Hill, "Differential thermal sensitivity of tumour and normal tissue microvascular response during hyperthermia," Int. J. Hyperthermia, **8**, 501–514 (1993).
[40]L. N. Dorr and K. Hynynen, "The effects of tissue heterogeneities and large vessels on the thermal exposure induced by short high-power ultrasound pulses," Int. J. Hyperthermia, **8**, 45–59 (1992).
[41]D. E. Haines, "The biophysics of radiofrequency catheter ablation in the heart: The importance of temperature monitoring," Pacing and Clinical Electrophysiology **16**(3pt2), 586–591 (1993).
[42]Gail ter Haar, "Ultrasound focal beam surgery," Ultrasound Med. Biol. **21**, 1089–1100 (1995).
[43]C. Damianou and K. Hynynen, "Focal spacing and near-field heating during pulsed high temperature ultrasound therapy," Ultrasound Med. Biol. **19**, 777–787, 1993.
[44]R. J. Lalonde, A. E. Worthington, and J. W. Hunt, "Field conjugate acoustic lenses for ultrasound hyperthermia," IEEE Trans. Ultrason. Ferroelect. Frequency Control **29**, 495–507 (1993).
[45]R. J. McGough, E. S. Ebbini, and C. A. Cain, "Direct computation of ultrasound phased-array driving signals from a specified temperature distribution for hyperthermia," IEEE Trans. Biomed. Eng. **39**, 825–835 (1992).
[46]J. C. Chato, "Heat transfer to blood vessels," J. Biomechan. Eng. **102**, 110–118 (1980).